Geophysical Research Letters

RESEARCH LETTER
10.1029/2019GL084974

Ocean Heat Content and the Intraseasonal Oscillation

A. V. Rydbeck[1], T. G. Jensen[1], T. A. Smith[1], M. K. Flatau[2], M. A. Janiga[2], C. A. Reynolds[2], and J. A. Ridout[2]

[1]U.S. Naval Research Laboratory, Stennis Space Center, Hancock, MS, USA, [2]U.S. Naval Research Laboratory, Monterey, CA, USA

Key Points:

- Over much of the Indian Ocean, ocean heat content increases as the intraseasonal oscillation amplifies
- The majority of intraseasonal ocean heat content variability is off equatorial (2°-10° latitude) and westward propagating
- Intraseasonal ocean heat content variations cannot be fully resolved by slab ocean models due to the effects of equatorial wave dynamics

Correspondence to:
A. V. Rydbeck,
adam.rydbeck@nrlssc.navy.mil

Citation:
Rydbeck, A. V., Jensen, T. G., Smith, T. A., Flatau, M. K., Janiga, M. A., Reynolds, C. A., & Ridout, J. A. (2019). Ocean heat content and the intraseasonal oscillation. *Geophysical Research Letters*, *46*. https://doi.org/10.1029/2019GL084974

Received 12 AUG 2019
Accepted 25 NOV 2019
Accepted article online 27 NOv 2019

Abstract Intraseasonal sea surface temperature anomalies generally cool during the convectively active phase of the intraseasonal oscillation in the Indian Ocean, but the behavior of intraseasonal ocean heat content anomalies is quite different. This is demonstrated using satellite observations and ocean reanalysis data. Ocean heat content anomalies increase during the convectively active phase of the intraseasonal oscillation and decrease during the convectively suppressed phase. Much of the intraseasonal variability of ocean heat content is westward propagating, moving in the opposite direction of the intraseasonal oscillation's convective envelope. While sea surface temperature anomalies are strongly regulated by variations in surface fluxes, their out of phase relationship with ocean heat content suggests that different processes are modulating the reservoir of warm water in the upper ocean. We hypothesize that oceanic equatorial waves are the primary forcing of intraseasonal ocean heat content anomalies during intraseasonal oscillation events.

Plain Language Summary The intraseasonal oscillation organizes rainfall in the tropics and often initiates over the Indian Ocean. It is associated with strong surface winds and widespread cloudiness, which decreases incoming solar radiation, resulting in a cooling of the sea surface. We observe that while the sea surface cools, the reservoir of warm water in the upper Indian Ocean actually increases. This seeming contradiction between the behavior of the sea surface temperature and the ocean heat content is explained by oceanic equatorial wave dynamics. Much of the ocean heat content variability moves westward along lines of latitude that are just poleward of the equator, consistent with the location, timing, and direction of equatorial Rossby wave propagation. By increasing the ocean heat content, these waves are hypothesized to reduce the amount of sea surface cooling produced by the intraseasonal oscillation.

1. Introduction

The intraseasonal oscillation (ISO) is characterized by strong air-sea interactions (DeMott et al., 2015, and references therein). Convectively active periods of the ISO manifest as vigorous surface zonal winds, deep atmospheric convection, and heavy precipitation with a horizontal expanse that covers most of the tropical Indian Ocean (Madden & Julian, 1971, 1972; Madden & Julian, 1994). During these periods, incoming solar radiation decreases, surface latent and sensible heat fluxes out of the ocean increase, and ocean mixing intensifies, resulting in a cooling of the ocean mixed layer and sea surface (Hendon et al., 1998; Moum et al., 2014; Shinoda et al., 1998). For the purpose of this investigation, we are interested in the upper ocean heat content (OHC), which characterizes the capacity of the ocean to mitigate the mixed layer cooling produced by the ISO.

During extended periods of intense atmospheric convection and strong winds in the tropics, OHC quantifies the warm water volume capable of supporting continued deep convection. OHC is commonly used to predict the behavior of tropical cyclones. Negative ocean feedbacks produced by tropical cyclones are sometimes thwarted in regions of high OHC, resulting in sustained or increased tropical cyclone strength (e.g., Halliwell et al., 2015; Shay et al., 2000; Shay & Brewster, 2010; Trenberth et al., 2018). Although surface winds are generally weaker during the ISO compared to tropical cyclones, they can endure for weeks (McPhaden, 1992; Zhang, 2005; Zhang & McPhaden, 2000), making the temporally integrated forcing comparable between the two phenomena. For example, at a fixed location, the wind stress forcing for 39 m/s winds that persist for 1 day is equivalent to 10 m/s winds that persist for 15 days. We propose that OHC is a useful metric for quantifying the oceanic resistance to cooling produced by turbulent mixing and surface heat fluxes.

The importance of OHC in the context of the ISO is emphasized in a recent study. Moum et al. (2016) hypothesized that the ISO can reduce the intensity of a subsequent ISO event by expending the OHC. In this scenario, the ocean governs the intensity of serial ISO events. Using in situ data from the DYNAMO experiment, it was observed that vertical mixing associated with shear instabilities at the base of the Yoshida-Wyrtki jet along the equator (Wyrtki, 1973; Yoshida, 1959) generated cooling that exceeded cooling from surface fluxes by 25%. The subsurface cooling forced by ocean dynamics persisted for an additional week after the wind forcing stopped, reflecting the ocean's ability to integrate and prolong atmospheric forcing. These results emphasize the important but often delayed impact of oceanic responses to ISO forcing.

While the study of Moum et al. (2016) investigated the negative feedback of OHC and the ISO along the equator, we expand the analysis area and reveal a positive feedback in off-equatorial regions whereby intraseasonal OHC increases during enhanced ISO convective phases. The behavior of OHC is opposite of the sea surface temperature (SST), such that OHC increases (decreases) when SST cools (warms). The responsible mechanism is, at present, not known, representing a gap in our understanding of intraseasonal air-sea interactions. This previously undocumented behavior is analyzed and a hypothesis is proposed. The relationship between intraseasonal OHC and convection anomalies within the ISO is examined using a combination of state-of-the-art ocean model reanalysis and satellite observations. The data and methods are described in section 2, results are shown in section 3, and conclusions are summarized in section 4.

2. Data and Methods

HYbrid Coordinate Ocean Model (HYCOM) reanalysis data from 1994 to 2015 is used to calculate the OHC. HYCOM has proven to successfully reproduce oceanic signatures of the ISO (i.e., Han et al., 2007; Rydbeck et al., 2017; Shinoda et al., 2008), and a summary of HYCOM reanalysis data is available in Rydbeck et al. (2019). In short, HYCOM has 41 vertical layers with a horizontal grid spacing of 0.08° (~9 km at the equator). The top 14 layers are fixed in sigma-z level space and confined to the upper 84 m. HYCOM surface forcing fields come from the National Centers for Environmental Prediction Climate Forecast System Reanalysis (Saha et al., 2010). The HYCOM reanalysis uses the Navy Coupled Data Assimilation system (NCODA; Cummings, 2006). NCODA is a fully three-dimensional, multivariate, variational ocean data assimilation scheme that integrates remotely sensed fields including sea surface height (SSH) and SST as well as in situ observations from platforms such as ships, buoys, expendable bathythermographs, CTDs, and Argo floats among others.

OHC in the tropics is often defined as the temperature excess above 26 °C integrated from the 26 °C isotherm to the surface (Leipper & Volgenau, 1972). This temperature threshold was originally selected because hurricanes do not typically form in regions of SST below 26 °C (Byers, 1959; Palmen, 1948). It was also suggested that because the mean surface air temperature of the tropics is near 26 °C (Malkus, 1972), air-sea interactions supportive of convection are generally suppressed in regions of SST cooler than 26 °C. More recent research has confirmed the 26 °C threshold for tropical convection (Bony et al., 1997; Lau et al., 1997; Zhang, 1993), and we use this as the threshold for integration in the formula:

$$\mathrm{OHC} = \rho c_p \int_{Z_{26^\circ\mathrm{C}}}^{\mathrm{Surface}} (T(z) - 299.15\ \mathrm{K})\partial z$$

where ρ is the density of seawater (1,027 kg m^{-3}), c_p is the specific heat of seawater at constant pressure (3,986 J kg^{-1} K^{-1}), $T(z)$ is the temperature in Kelvin as a function of depth, and $Z_{26\,^\circ\mathrm{C}}$ is the depth of the 26 °C isotherm. OHC units are shown in kJ cm^{-2}.

SSTs from the National Oceanic and Atmospheric Administration daily optimum interpolation V2 (0.25° grid spacing) that includes a combination of Advanced Very High Resolution Radiometer and Advanced Microwave Scanning Radiometer-Earth observing system are utilized (Reynolds et al., 2007). The National Climatic Data Center outgoing longwave radiation (OLR) daily climate data record (1° grid spacing) is used as a proxy for atmospheric convection (Lee, 2014).

For the purposes of this study, the ISO phase and amplitude are defined by the OLR Madden-Julian Oscillation Index (OMI) (Kiladis et al., 2014). Because we are interested in variations of OHC associated with the austral summer Madden-Julian Oscillation and boreal summer intraseasonal oscillation, the OMI

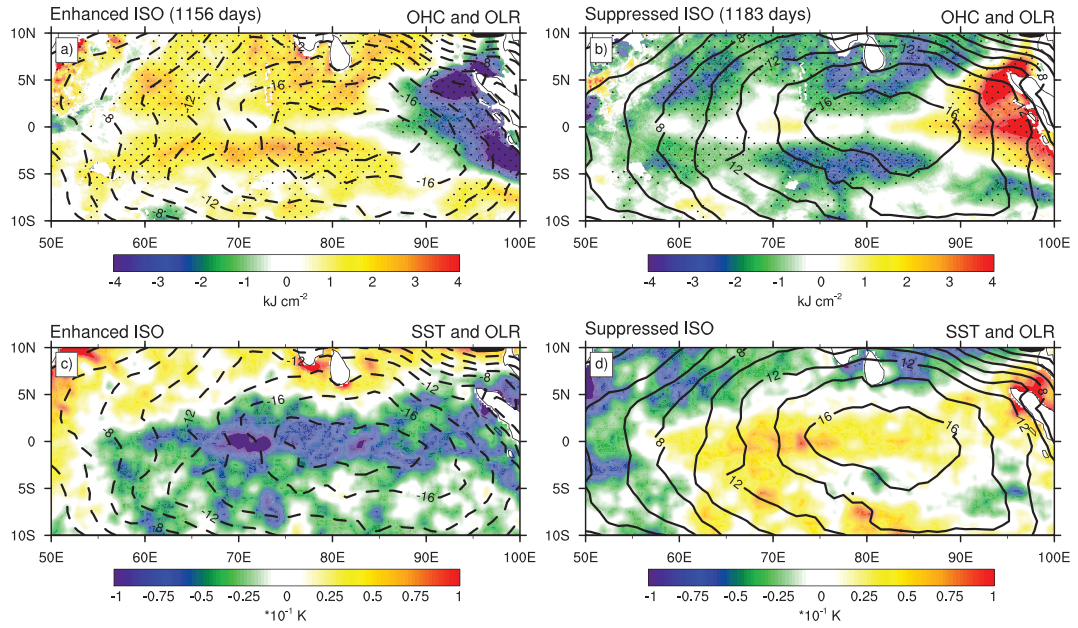

Figure 1. Composite of intraseasonal OLR anomalies during ISO enhanced (a, c) and suppressed (b, d) phases in the Indian Ocean. Intraseasonal OHC anomalies (shading; kJ cm^{-2}) are shown in (a) and (b). Intraseasonal SST anomalies (shading; $\times 10^{-1}$ K) are shown in (c) and (d). Negative (positive) OLR anomalies are dashed (solid) with contour interval every 2 W m^{-2}. The number of days included in the respective phases are shown above (a) and (b). Black stippling in (a) and (b) indicate regions where OHC anomalies are significantly different between the ISO suppressed and enhanced phases at the 99% confidence threshold using a two-tailed student's *t* test.

represents the respective eastward and poleward propagating components of both intraseasonal modes with much greater fidelity than alternative intraseasonal indices (Wang et al., 2018). OMI information from 1994 to 2015 is used to create all season composite maps. Days with an OMI amplitude greater than 1.5 standard deviations are used for compositing. Intraseasonal anomalies of atmospheric and oceanic fields shown in composites are calculated by removing the first three harmonics of the seasonal cycle and then bandpass filtering with a Lanzcos filter to retain variability with 30–150 day periods.

3. Results

Intraseasonal composites of OHC, OLR, and SST anomalies are shown in Figure 1 as a function of ISO convective phase in the Indian Ocean. During the enhanced convective phase (phases 1–4), OHC anomalies are positive in the off-equatorial western and central Indian Ocean (Figure 1a). Drawing on conventional wisdom, one might expect negative OHC anomalies to be present since the enhanced convective phase of the MJO is associated with strong westerly wind stress anomalies, reduced incoming solar radiation, and increased surface latent heat fluxes. The behavior of SST anomalies, which are cool along the equator, is consistent with such surface forcing mechanisms and the Yoshida-Wyrtki jet induced cooling described by Moum et al. (2016) (Figure 1c). The OHC and SST anomalies are predominantly out-of-phase in the region 5°N–10°S, 55°–85°E. We will discuss a possible mechanism for this previously undocumented behavior later in the section.

During periods when ISO convection in the Indian Ocean is suppressed (phases 5–8), OHC anomalies are negative over much of the western and central Indian Ocean (Figure 1b). These periods are characterized by enhanced incoming solar radiation, reduced wind stress anomalies, reduced latent heat fluxes, and a general warming of the sea surface along the equator and coast of Sumatra (Figure 1d). An exception to the contradictory behavior between OHC and SST occurs in the eastern Indian Ocean where anomalies are mostly in-phase; positive OHC anomalies occur during suppressed conditions and negative OHC anomalies occur during enhanced conditions. For much of the Indian Ocean, OHC anomalies between the respective ISO convective phases are significantly different at the 99% confidence threshold. We hypothesize that oceanic equatorial waves are responsible for the largely out-of-phase relationship between OHC and SST

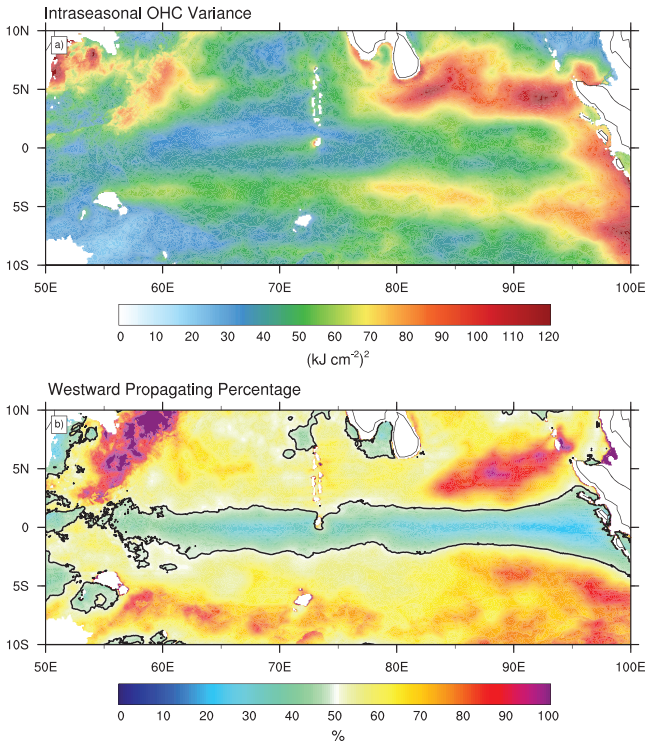

Figure 2. Intraseasonal OHC variance ((kJ cm^{-2})^2) is shown in (a). The percentage of intraseasonal OHC variance that is westward propagating is shown in (b). The latter is calculated by filtering the intraseasonal OHC anomalies for wave numbers less than or equal to −1 (i.e., westward propagating waves) and calculating the variance. The wave number filtered variance is then used to calculate the percentage of total variance that is westward propagating. The black line in (b) indicates the 50% contour. The stationary/eastward propagating percentage is defined as 100% less the westward propagating percentage.

anomalies in regions of the western and central Indian Ocean and the in-phase relationship between the two in the eastern Indian Ocean.

Figure 2 shows the intraseasonal variance of OHC and the percentage of intraseasonal variance that is westward propagating. The major centers of intraseasonal OHC variability extend from the eastern to central Indian Ocean along 5°N and 5°S. Variance in the northern band is 25–40% greater than that in the southern band between 75 and 95°E. The variance in the northern band is partly related to the southwest monsoon current located near the southeastern coast of Sri Lanka (Hastenrath & Greischar, 1991) and the northwestward tilt of the Sumatra coastline that can focus ocean energy in the region. The region of 4–10°N, 50–55° E is also characterized by high OHC variance but is limited by the climatologically cool upper ocean in the far western Indian Ocean. Given the eastward propagation of ISO winds, surface fluxes, and convection, it might be expected that OHC anomalies should also propagate eastward. However, as evidenced by the percentage of intraseasonal OHC variance associated with the westward propagation of OHC anomalies in Figure 2b, only a small area of OHC variance is dominated by eastward propagating and stationary variability. Most off-equatorial maxima of intraseasonal OHC variance are characterized by westward propagation. These are also well-known regions of westward propagating equatorial Rossby waves linked to the ISO (Jensen et al., 2015; Rydbeck et al., 2017; Rydbeck & Jensen, 2017; Shinoda et al., 2013, 2017; Webber et al., 2010; Webber et al., 2012; Webber et al., 2012; West et al., 2018). High percentages in the northern hemisphere of the western Indian Ocean are likely related to variability that anticyclonically orbits the Great Whirl (e.g., Melzer et al., 2019; Schott et al., 1990). The narrow region along the equator between 2°S and 2°N across the Indian Ocean is typically characterized by strong eastward propagating Yoshida-Wyrtki jets and oceanic Kelvin waves forced by ISO wind stress anomalies similar to intraseasonal variability observed in Moum et al. (2016).

The off-equatorial response of OHC anomalies to the ISO in the western and central Indian Ocean suggests that surface flux processes, to first order, are not responsible for the phase locking of intraseasonal convection and the off-equatorial reservoir of upper ocean heat there. We hypothesize that alternative mechanisms beyond simple atmospheric forcing are responsible for these patterns of intraseasonal OHC variability. While previous studies have examined the intraseasonal patterns of SST and ocean mixed layer temperature, OHC on these timescales has received little attention. We hypothesize that intraseasonal OHC variability shown in Figures 1 and 2 corresponds to oceanic equatorial wave propagation wherein eastward propagating waves along the equator and westward propagating waves poleward of the equator govern intraseasonal OHC variability.

To investigate the evolving relationship between ISO convection and OHC anomalies, we examine composite maps of them as a function of ISO phase (Figure 3). Negative OLR anomalies enter the western Indian Ocean in Phase 1 and are associated with positive OHC anomalies located just poleward of the equator across much of the Indian Ocean. A narrow band of negative OHC anomalies is located along the equator and spans the entire basin. In Phase 2, enhanced convection covers most of the Indian Ocean and positive OHC anomalies persist just poleward of the equator. The equatorial band of negative OHC anomalies has largely relaxed except in the eastern basin near Sumatra where negative OHC anomalies extend poleward along the coast. In Phase 3, positive OHC anomalies cover most of the central and western Indian Ocean including along the equator, while negative OHC anomalies in the eastern Indian Ocean are separated into local maxima centered along 4°S and 4°N. In Phase 4, positive OHC anomalies are located along the equator and negative anomalies develop in the off-equatorial regions. The local negative maxima in the eastern side of the basin have propagated slightly westward. Enhanced convection weakens during this phase as convectively suppressed conditions become dominant in Phase 5. The positive OHC anomalies have intensified

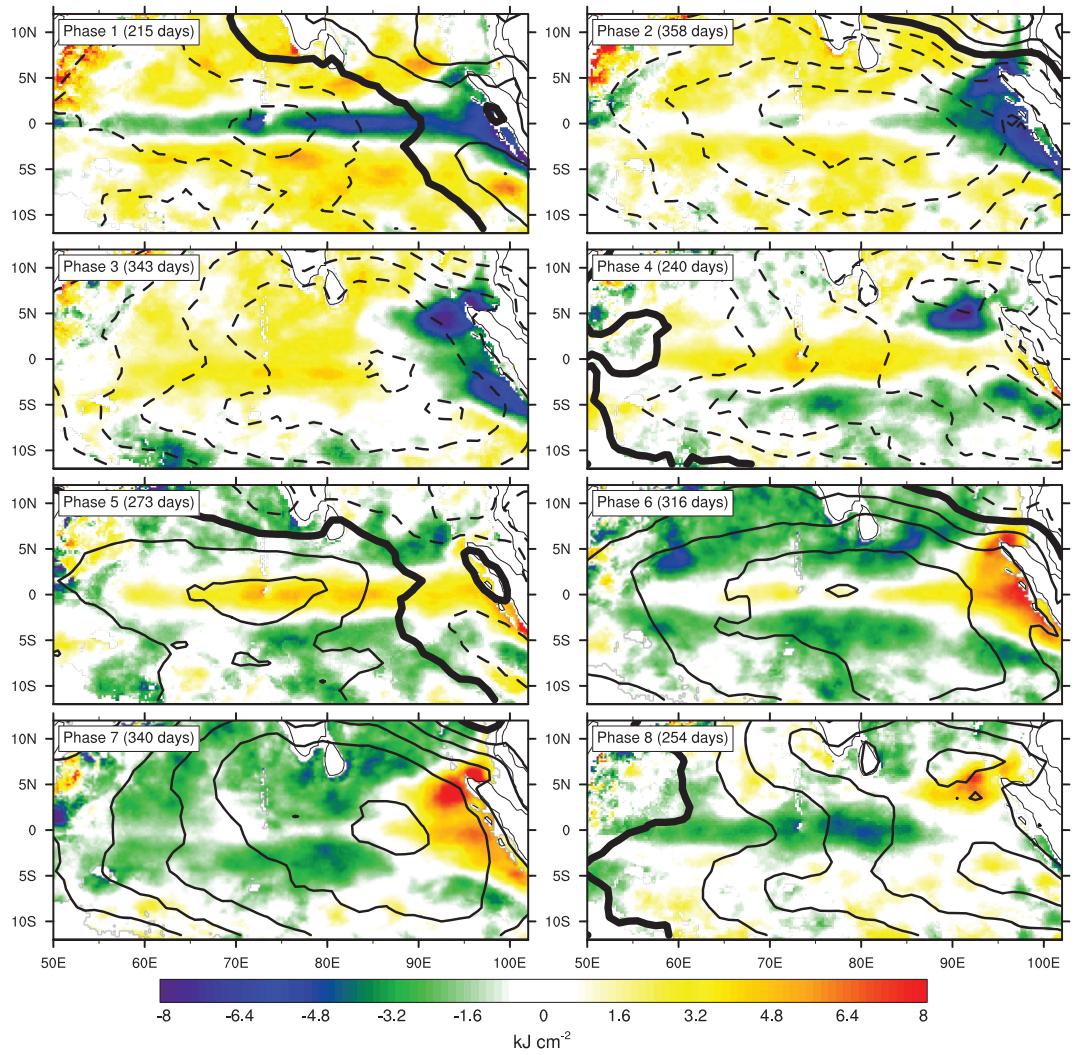

Figure 3. ISO composite of intraseasonal OHC (shading: kJ cm^{-2}) and OLR (contours; W m^{-2}) anomalies. Negative (positive) OLR anomalies are dashed (solid) with contour interval every 2 W m^{-2}. The black thick line indicates 0 W m^{-2}. The phase number and total number of days used in each phase composite are shown in the upper left of each panel.

toward the eastern Indian Ocean in Phase 5, while negative OHC anomalies in the off-equatorial region continue to strengthen along 5°S and 5°N. In Phases 6 and 7, positive OHC anomalies along the equator weaken but appear to reflect off the coast of Sumatra into local maxima with the strongest located at 4°N, similar to the evolution of local OHC minima in Phase 4. Negative OHC anomalies weaken in off-equatorial regions while intensifying on the equator in Phase 8 at which time the whole cycle repeats. To note, the weak OHC anomalies along the equator during enhanced and suppressed phases in Figure 1 are a result of averaging large but oppositely signed anomalies in Phases 1–4 and 5–8.

The reflection of OHC anomalies on the eastern side of the basin is analogous to the reflection of Kelvin waves into poleward propagating coastal Kelvin waves and westward propagating equatorial Rossby waves (e.g., Rydbeck & Jensen, 2017; Webber et al., 2010; Webber, Matthews, et al., 2012; Webber, Stevens, et al., 2012). Downwelling (upwelling) waves depress (shoal) isotherms, increasing (decreasing) the upper ocean warm water volume. OHC anomalies are forced by changes to the layer temperature and/or layer thickness. The patterns of 26 °C isotherm depth anomalies (not shown) match those of OHC suggesting important roles for downwelling and upwelling oceanic waves that depress and shoal the 26 °C isotherm, modulating the layer thickness. The phase speed of the first baroclinic mode oceanic Kelvin wave is ~2.7 m/s, and the equatorial Rossby wave phase speed is ~1/3 (0.9 m/s) of the Kelvin wave. The roughly 30 and 90 day periods of

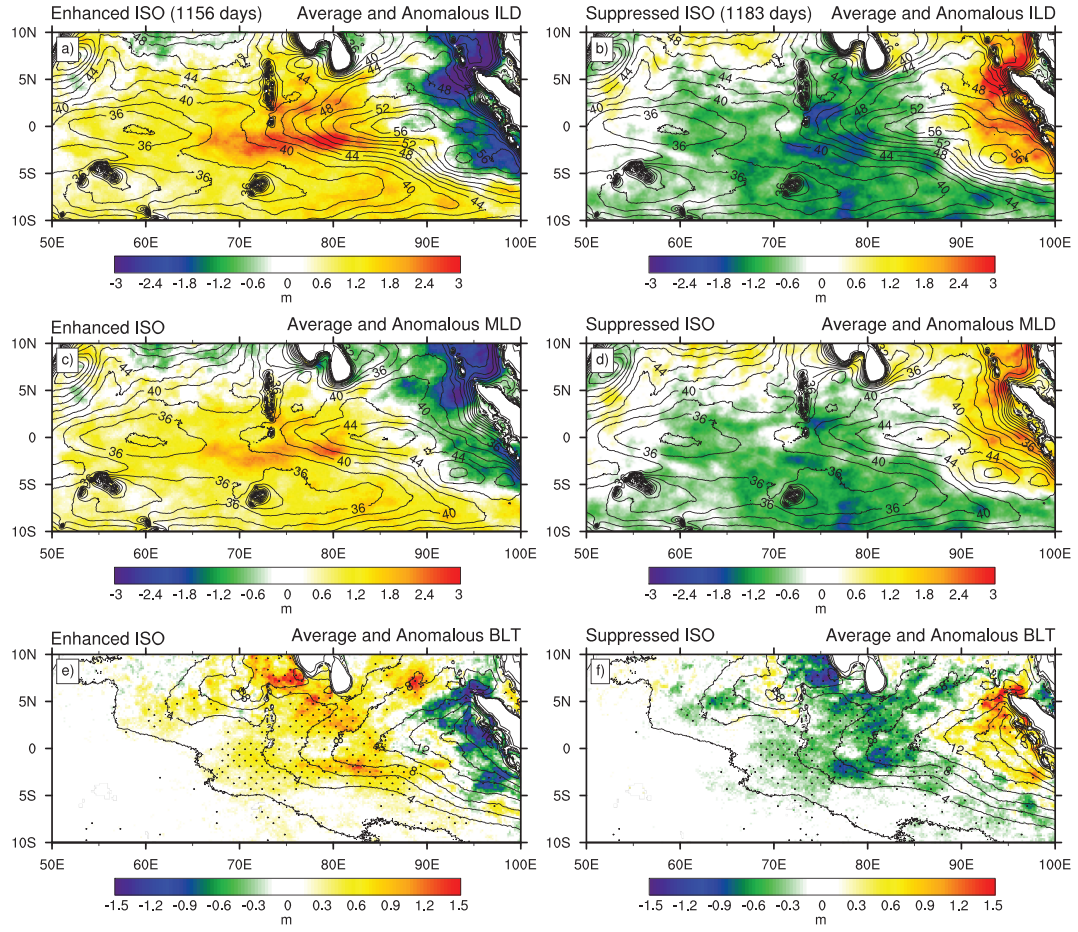

Figure 4. Composites of intraseasonal ILD (a, b), MLD (c, d), and BLT (e, f) anomalies during ISO enhanced (a,c,d) and suppressed (b, d, and f) phases are shown using the shaded contours. The respective mean ILD, MLD, and BLT (m) are shown using line contours with a 2 m contour interval. The number of days included in the composites are shown above (a) and (b). Black stippling in (e) and (f) indicate regions where the enhanced and suppressed ISO BLT anomalies are significantly different at the 99% confidence threshold using a two-tailed student's *t* test.

these waves in the Indian Ocean likely explains the imperfect projection of their characteristics onto the 45 day periods of the ISO in the composite. This might cause the waves to appear jumpy or overly smoothed in the phase composites, obscuring their true phase evolution. Nonetheless, Figure 3 suggests that Kelvin waves along the equator transport OHC anomalies eastward while equatorial Rossby waves in the off-equatorial regions transport OHC westward. We hypothesize that the development of new Rossby waves in the eastern Indian Ocean and the propagation of oppositely signed waves in the central and western Indian Ocean explains the zonally out of phase OHC anomalies in Figure 1. The Rossby waves in the central and western Indian Ocean favorably synchronize with ISO convection.

An additional factor that can mitigate mixed layer cooling produced by ISO induced ocean turbulent mixing and surface heat fluxes relates to the vertical stratification of the upper ocean. When warm salty water is overlaid by warm fresh water, barrier layers form and insulate the mixed layer from the relatively cool ocean below (e.g., Drushka et al., 2014; Girishkumar et al., 2011; Sprintall & Tomczak, 1992). Barrier layer thickness (BLT) is defined as the difference between the mixed layer depth (MLD) and the isothermal layer depth (ILD) and is used as a proxy to quantify the degree of upper ocean stratification. Thick barrier layers represent increased stratification such that they resist mixing effects, while the reduction of BLT diminishes the vertical stratification making the mixed layer more vulnerable to cooling by mixing. The MLD and ILD are calculated using HYCOM reanalysis data with the fixed density criterion of 0.125 kg m^{-3} referenced from 10 m for the MLD and the corresponding temperature change of 0.35 K referenced from 10 m for the ILD.

The anomalous (shading) and average (contours) ILD, MLD, and BLT fields are shown in Figure 4 during enhanced and suppressed ISO phases. We are interested in determining if oceanic equatorial waves that feature prominently in intraseasonal OHC variability also manifest in ocean stratification variability as indicated by intraseasonal BLT anomalies. In the central Indian Ocean the ILD deepens by ~3 m during enhanced ISO convection and shoals by ~2 m during suppressed ISO convection. Similar to OHC, the anomalies in the eastern Indian Ocean are out of phase with those in the central Indian Ocean, perhaps resulting from the propagation of oppositely signed (upwelling versus downwelling) equatorial waves. The pattern of MLD anomalies shown in Figures 4c and 4d is similar to that of the ILD but the amplitudes are slightly weaker.

The BLT anomalies shown in Figures 4e and 4f are positive during enhanced ISO convective phases and negative during suppressed ISO convective phases in the central Indian Ocean. The thickening of the barrier layer by ~1 m strengthens the mixed layer's resistance to cooling by mechanical mixing at its base. Periods of enhanced ISO convection are associated with an off-equatorial increase of thermodynamic insulation resulting from the combined effects of increased BLT and OHC. While these processes are not sufficient to entirely prevent surface cooling during the convectively enhanced ISO phase (see Figure 1c), they perhaps retard the rate of cooling within the mixed layer. In the eastern Indian Ocean, the BLT decreases (increases) during convectively enhanced (suppressed) periods and is in phase with SST anomalies there. The east-west dipole character of the intraseasonal BLT anomalies is similar to that of OHC anomalies, suggesting that mechanisms responsible for OHC anomalies may also force BLT anomalies. In the eastern Indian Ocean, the phase alignment of OHC, BLT, and SST anomalies suggests that subsurface ocean properties are reinforcing the SST tendency. The exact magnitude of the effect of OHC and BLT anomalies in this region is difficult to interpret from the present analysis since the climatological OHC of the eastern Indian Ocean is high (not shown) and the climatological barrier layer is thick.

One possible mechanism for the creation of BLT anomalies in the central Indian Ocean relates to horizontal advection. The amplitudes of the ILD, MLD, and BLT anomalies in the central Indian Ocean tend to maximize in regions of strong climatological horizontal gradients. Because the climatological ILD gradients are stronger in the equatorial Indian Ocean than those of the MLD, anomalous intraseasonal currents advecting along these gradients would generate a larger anomaly in ILD than MLD, thus creating a BLT anomaly. This suggests that equatorial wave dynamics associated with anomalous currents might play a role in the development of BLT anomalies. Future work is required to precisely determine the importance of this process and others, such as precipitation and vertical mixing, to the growth of intraseasonal BLT anomalies in the central Indian Ocean.

4. Conclusions

Off-equatorial intraseasonal OHC anomalies increase in the central and western Indian Ocean during periods of enhanced intraseasonal convection, in opposition to conventional wisdom, which suggests that OHC should decrease in the same manner that SST cools during these periods. The dominant processes which determine the phase and magnitude of SST anomalies do not appear to control the OHC anomalies. Off-equatorial intraseasonal OHC anomalies chiefly propagate westward, opposite to the direction of ISO convective propagation. We hypothesize that subsurface ocean dynamics driven by oceanic equatorial waves govern the development of positive OHC anomalies during the enhanced phase of the ISO.

The circulation of intraseasonal OHC anomalies in the Indian Ocean begins along the equator where they propagate eastward, reflect at the eastern boundary of the basin, propagate westward along 5° latitude into the central and western Indian Ocean, and finally develop again along the equator to complete the circuit. OHC anomalies in the eastern Indian Ocean are typically out of phase with those in the western and central Indian Ocean, which is perhaps a result of contrasting wave types and phases (upwelling versus downwelling) simultaneously occurring in different regions of the Indian Ocean. The circulation of OHC anomalies during ISO events agrees with the preferred latitudes and directions of propagation of first baroclinic mode equatorial Kelvin and Rossby waves, supporting the hypothesis that ocean dynamics govern the magnitude and phase of intraseasonal OHC anomalies. Similar to the patterns of OHC anomalies, the barrier layer thickens (thins) in the central Indian Ocean during enhanced (suppressed) ISO convection.

Atmospheric models coupled to slab ocean models will not be able to capture the phase, propagation, and magnitude of intraseasonal OHC and BLT anomalies resulting from oceanic equatorial wave dynamics. Our results suggest that wave dynamics are likely a leading contributor to the manifestation of OHC and BLT anomalies, indicating that full physics ocean models are required to appropriately resolve subsurface intraseasonal variability.

Acknowledgments
Funding is provided by the NRL Karle's Fellowship, ONR PISTON, and ONR MISO-BoB projects. NOAA SST (http://www.ncdc.noaa.gov/oisst) and NCDC OLR (https://www.ncdc.noaa.gov/cdr/atmospheric/outgoing-longwave-radiation-daily) is provided by NCEI. HYCOM + NCODA reanalysis is stored at the Navy DoD Supercomputing Resource Center (DSRC). Access to the DSRC may be obtained through a request to the DoD High Performance Computer Modernization Program (https://www.hpc.mil/). Once an account has been established, the corresponding author may be contacted for information to access the archived data.

References

Bony, S., Lau, K. M., & Sud, Y. C. (1997). Sea surface temperature and large-scale circulation influences on tropical greenhouse effect cloud radiative forcing. *Journal of Climate*, *10*(8), 2055–2077. https://doi.org/10.1175/1520-0442(1997)010<2055:SSTALS>2.0.CO;2

Byers, H. R. (1959). *General meteorology* (Vol. 86). New York: McGraw-Hill. https://doi.org/10.1002/qj.49708636716

Cummings, J. A. (2006). Operational multivariate ocean data assimilation. *Quarterly Journal of the Royal Meteorological Society*, *131*(613), 3583–3604. https://doi.org/10.1256/qj.05.105

DeMott, C. A., Klingaman, N. P., & Woolnough, S. J. (2015). Atmosphere-ocean coupled processes in the Madden-Julian oscillation. *Reviews of Geophysics*, *53*, 1099–1154. https://doi.org/10.1002/2014RG000478

Drushka, K., Sprintall, J., & Gille, S. T. (2014). Subseasonal variations in salinity and barrier-layer thickness in the eastern equatorial Indian Ocean. *Journal of Geophysical Research: Oceans*, *119*, 805–823. https://doi.org/10.1002/2013JC009422

Girishkumar, M. S., Ravichandran, M., McPhaden, M. J., & Rao, R. R. (2011). Intraseasonal variability in barrier layer thickness in the south central Bay of Bengal. *Journal of Geophysical Research*, *116*, C03009. https://doi.org/10.1029/2010JC006657

Halliwell, G. R., Gopalakrishnan, S., Marks, F., & Willey, D. (2015). Idealized study of ocean impacts on tropical cyclone intensity forecasts. *Monthly Weather Review*, *143*(4), 1142–1165. https://doi.org/10.1175/mwr-d-14-00022.1

Han, W., Yuan, D., Liu, W. T., & Halkides, D. J. (2007). Intraseasonal variability of Indian Ocean sea surface temperature during boreal winter: Madden-Julian Oscillation versus submonthly forcing and processes. *Journal of Geophysical Research*, *112*, C04001. https://doi.org/10.1029/2006JC003791

Hastenrath, S., & Greischar, L. (1991). The monsoonal current regimes of the tropical Indian Ocean: Observed surface flow fields and their geostrophic and wind-driven components. *Journal of Geophysical Research*, *96*(C7), 12619. https://doi.org/10.1029/91jc00997

Hendon, H. H., Liebmann, B., & Glick, J. D. (1998). Oceanic Kelvin waves and the Madden–Julian Oscillation. *Journal of the Atmospheric Sciences*, *55*(1), 88–101. https://doi.org/10.1175/1520-0469(1998)055<0088:OKWATM>2.0.CO;2

Jensen, T. G., Shinoda, T., Chen, S., & Flatau, M. (2015). Ocean response to CINDY/DYNAMO MJOs in air-sea-coupled COAMPS. *Journal of the Meteorological Society of Japan. Ser. II*, *93A*, 157–178. https://doi.org/10.2151/jmsj.2015-049

Kiladis, G. N., Dias, J., Straub, K. H., Wheeler, M. C., Tulich, S. N., Kikuchi, K., et al. (2014). A Comparison of OLR and circulation-based indices for tracking the MJO. *Monthly Weather Review*, *142*(5), 1697–1715. https://doi.org/10.1175/MWR-D-13-00301.1

Lau, K. M., Wu, H. T., & Bony, S. (1997). The role of large-scale atmospheric circulation in the relationship between tropical convection and sea surface temperature. *Journal of Climate*, *10*(3), 381–392. https://doi.org/10.1175/1520-0442(1997)010<0381:TROLSA>2.0.CO;2

Lee, H.-T. (2014). *Climate Algorithm Theoretical Basis Document (C-ATBD): Outgoing longwave radiation (OLR)—Daily*. Retrieved from http://www1.ncdc.noaa.gov/pub/data/sds/cdr/CDRs/Outgoing Longwave Radiation-Daily/AlgorithmDescription.pdf.

Leipper, D. F., & Volgenau, D. (1972). Hurricane heat potential of the Gulf of Mexico. *Journal of Physical Oceanography*, *2*(3), 218–224. https://doi.org/10.1175/1520-0485(1972)002<0218:hhpotg>2.0.co;2

Madden, R., & Julian, P. (1994). Observations of the 40-50 day tropical oscillation a review. *Monthly Weather Review*, *122*(5), 814–837. Retrieved from http://journals.ametsoc.org/doi/abs/10.1175/1520-0493(1994)122%3C0814:OOTDTO%3E2.0.CO;2

Madden, R. A., & Julian, P. R. (1971). Detection of a 40–50 day oscillation in the zonal wind in the tropical Pacific. *Journal of the Atmospheric Sciences*, *28*(5), 702–708. https://doi.org/10.1175/1520-0469(1971)028<0702:DOADOI>2.0.CO;2

Madden, R. A., & Julian, P. R. (1972). Description of global-scale circulation cells in the tropics with a 40–50 day period. *Journal of the Atmospheric Sciences*, *29*(6), 1109–1123. https://doi.org/10.1175/1520-0469(1972)029<1109:DOGSCC>2.0.CO;2

Malkus, J. S. (1972). Large-scale interactions. In *The sea* (1st ed., pp. 86–322). New York: Wiley.

McPhaden, M. J. (1992). The response of the western equatorial Pacific Ocean to westerly wind bursts during November 1989 to January 1990. *Journal of Geophysical Research*, *97*(C9), 14289. https://doi.org/10.1029/92jc01197

Melzer, B. A., Jensen, T. G., & Rydbeck, A. V. (2019). Evolution of the great whirl using an altimetry-based eddy tracking algorithm. *Geophysical Research Letters*, *46*(8), 4378–4385. https://doi.org/10.1029/2018GL081781

Moum, J. N., Pujiana, K., Lien, R. C., & Smyth, W. D. (2016). Ocean feedback to pulses of the Madden-Julian Oscillation in the equatorial Indian Ocean. *Nature Communications*, *7*, 13203. https://doi.org/10.1038/ncomms13203

Moum, J. N., de Szoeke, S. P., Smyth, W. D., Edson, J. B., DeWitt, H. L., Moulin, A. J., et al. (2014). Air-sea interactions from westerly wind bursts during the November 2011 MJO in the Indian Ocean. *Bulletin of the American Meteorological Society*, *95*(8), 1185–1199. https://doi.org/10.1175/BAMS-D-12-00225.1

Palmen, E. (1948). On the formation and structure of tropical hurricanes. *Geophysica*, *3*, 26–38. Retrieved from http://www.geophysica.fi/pdf/geophysica_1948_3_1_026_palmen.pdf

Reynolds, R. W., Smith, T. M., Liu, C., Chelton, D. B., Casey, K. S., & Schlax, M. G. (2007). Daily high-resolution-blended analyses for sea surface temperature. *Journal of Climate*, *20*(22), 5473–5496. https://doi.org/10.1175/2007JCLI1824.1

Rydbeck, A. V., Jensen, T. G., & Flatau, M. (2019). Characterization of intraseasonal Kelvin waves in the equatorial Pacific Ocean. *Journal of Geophysical Research: Oceans*, *124*, 2028–2053. https://doi.org/10.1029/2018JC014838

Rydbeck, A. V., & Jensen, T. G. (2017). Oceanic impetus for convective onset of the Madden-Julian oscillation in the western Indian ocean. *Journal of Climate*, *30*(11), 4299–4316. https://doi.org/10.1175/JCLI-D-16-0595.1

Rydbeck, A. V., Jensen, T. G., & Nyadjro, E. S. (2017). Intraseasonal sea surface warming in the western Indian Ocean by oceanic equatorial Rossby waves. *Geophysical Research Letters*, *44*, 4224–4232. https://doi.org/10.1002/2017GL073331

Saha, S., Moorthi, S., Pan, H. L., Wu, X., Wang, J., Nadiga, S., et al. (2010). The NCEP climate forecast system reanalysis. *Bulletin of the American Meteorological Society*, *91*(8), 1015–1057. https://doi.org/10.1175/2010BAMS3001.1

Schott, F., Swallow, J. C., & Fieux, M. (1990). The Somali current at the equator: Annual cycle of currents and transports in the upper 1000 m and connection to neighbouring latitudes. *Deep Sea Research Part A, Oceanographic Research Papers*, *37*(12), 1825–1848. https://doi.org/10.1016/0198-0149(90)90080-F

Shay, L. K., & Brewster, J. K. (2010). Oceanic heat content variability in the Eastern Pacific Ocean for hurricane intensity forecasting. *Monthly Weather Review*, *138*(6), 2110–2131. https://doi.org/10.1175/2010mwr3189.1

Shay, L. K., Goni, G. J., & Black, P. G. (2000). Effects of a warm oceanic feature on Hurricane Opal. *Monthly Weather Review*, *128*(5), 1366–1383. https://doi.org/10.1175/1520-0493(2000)128<1366:eoawof>2.0.co;2

Shinoda, T., Han, W., Zamudio, L., Lien, R. C., & Katsumata, M. (2017). Remote ocean response to the Madden-Julian oscillation during the DYNAMO field campaign: Impact on Somali current system and the Seychelles-Chagos thermocline ridge. *Atmosphere*, *8*(9), 171. https://doi.org/10.3390/atmos8090171

Shinoda, T., Hendon, H. H., & Glick, J. (1998). Intraseasonal variability of surface fluxes and sea surface temperature in the tropical Western Pacific and Indian Oceans. *Journal of Climate*, *11*(7), 1685–1702. https://doi.org/10.1175/1520-0442(1998)011<1685:IVOSFA>2.0.CO;2

Shinoda, T., Jensen, T. G., Flatau, M., Chen, S., Han, W., & Wang, C. (2013). Large-scale oceanic variability associated with the Madden-Julian Oscillation during the CINDY/DYNAMO field campaign from satellite observations. *Remote Sensing*, *5*(5), 2072–2092. https://doi.org/10.3390/rs5052072

Shinoda, T., Roundy, P. E., & Kiladis, G. N. (2008). Variability of intraseasonal Kelvin waves in the equatorial pacific ocean. *Journal of Physical Oceanography*, *38*(5), 921–944. https://doi.org/10.1175/2007JPO3815.1

Sprintall, J., & Tomczak, M. (1992). Evidence of the barrier layer in the surface layer of the tropics. *Journal of Geophysical Research*, *97*(C5), 7305. https://doi.org/10.1029/92jc00407

Trenberth, K. E., Cheng, L., Jacobs, P., Zhang, Y., & Fasullo, J. (2018). Hurricane Harvey links to ocean heat content and climate change adaptation. *Earth's Future*, *6*(5), 730–744. https://doi.org/10.1029/2018EF000825

Wang, S., Ma, D., Sobel, A. H., & Tippet, M. K. (2018). Propagation characteristics of BSISO indices. *Geophysical Research Letters*. https://doi.org/10.1029/2018GL078321

Webber, B. G. M., Matthews, A. J., & Heywood, K. J. (2010). A dynamical ocean feedback mechanism for the Madden-Julian Oscillation. *Quarterly Journal of the Royal Meteorological Society*, *136*(648), 740–754. https://doi.org/10.1002/qj.604

Webber, B. G. M., Matthews, A. J., Heywood, K. J., & Stevens, D. P. (2012). Ocean Rossby waves as a triggering mechanism for primary Madden-Julian events. *Quarterly Journal of the Royal Meteorological Society*, *138*(663), 514–527. https://doi.org/10.1002/qj.936

Webber, B. G. M., Stevens, D. P., Matthews, A. J., & Heywood, K. J. (2012). Dynamical ocean forcing of the Madden-Julian oscillation at lead times of up to five months. *Journal of Climate*, *25*(8), 2824–2842. https://doi.org/10.1175/JCLI-D-11-00268.1

West, B. J., Han, W., & Li, Y. (2018). The role of oceanic processes in the initiation of Indian summer monsoon intraseasonal oscillations over the Indian Ocean. *Journal of Geophysical Research: Oceans*, *123*, 3685–3704. https://doi.org/10.1029/2017JC013564

Wyrtki, K. (1973). An equatorial jet in the Indian Ocean. *Science*, *181*(4096), 262–264. https://doi.org/10.1126/science.181.4096.262

Yoshida, K. (1959). A theory of the Cromwell Current (the equatorial undercurrent) and of the equatorial upwelling. *Journal of the Oceanographical Society of Japan*, *15*(4), 159–170. https://doi.org/10.5928/kaiyou1942.15.159

Zhang, C. (1993). Large-scale variability of atmospheric deep convection in relation to sea surface temperature in the tropics. *Journal of Climate*, *6*(10), 1898–1913. https://doi.org/10.1175/1520-0442(1993)006<1898:lsvoad>2.0.co;2

Zhang, C. (2005). Madden-Julian Oscillation. *Reviews of Geophysics*. https://doi.org/10.1029/2004RG000158

Zhang, C., & McPhaden, M. J. (2000). Intraseasonal surface cooling in the equatorial western Pacific. *Journal of Climate*, *13*(13), 2261–2276. https://doi.org/10.1175/1520-0442(2000)013<2261:ISCITE>2.0.CO;2